ICES Journal of Marine Science

ICES Journal of Marine Science (2019), 76(4), 1177–1188. doi:10.1093/icesjms/fsz005

Original Article

Scaling of size, shape and surface roughness in Antarctic krill swarms

Alexey B. Ryabov[1] and Geraint A. Tarling [2]*

[1]Institute for Chemistry and Biology of the Marine Environment, University of Oldenburg, Oldenburg 26111, Germany
[2]British Antarctic Survey, Natural Environment Research Council, High Cross, Madingley Road, Cambridge CB3 0ET, UK

*Corresponding author: tel: +44 (0)1223 221596; e-mail: gant@bas.ac.uk.

Ryabov, A. B. and Tarling, G. A. Scaling of size, shape and surface roughness in Antarctic krill swarms. – ICES Journal of Marine Science, 76: 1177–1188.

Received 16 October 2018; revised 20 December 2018; accepted 10 January 2019; advance access publication 2 February 2019.

Antarctic krill are obligate swarmers and the size and shape of the swarms they form can have a major influence on trophic interactions and biogeochemical fluxes. Parameterizing variability in size and shape is therefore a useful step toward understanding the operation of the Southern Ocean ecosystem. We analyse the relationships between the length L, thickness T, perimeter P, and area A of 4650 vertical cross-sections of open-ocean krill swarms obtained within the Atlantic sector of the Southern Ocean in summer 2003. Our data show that these parameters are tightly interrelated. The thickness T increases on average as $L^{0.67}$ and has a log-normal distribution within each length class. The perimeter and area scale with L and T as $P \sim L^{0.77}T$ and $A \sim L^{0.86}T^{0.48}$. The swarm aspect ratio, T/L, decreases approximately as $L^{-0.32}$. The surface roughness (defined as P/A) has a weak dependence on swarm length and decreases approximately as $T^{-0.46}$, which can be explained only by the appearance of indentations and cavities in the swarm shape. Overall, our study finds that there are distinct limits to the size and shape of swarms that Antarctic krill appear to be capable of forming and we explore the potential explanatory factors contributing to these limitations.

Keywords: acoustics, area, aspect ratio, *Euphausia superba*, perimeter, Scotia Sea, Southern Ocean.

Introduction

Swarms of Antarctic krill (*Euphausia superba* Dana, hereon: krill) vary enormously from lengths of just a few metres to several kilometres and vertical thicknesses of over 100 m (Siegel and Kalinowski, 1994; Tarling *et al.*, 2009; Krafft *et al.*, 2012). These variations are accompanied by corresponding changes in other parameters, such as perimeter and area in two dimensions, and surface area and volume in three dimensions, which together define external swarm shape. The shape of a swarm is a function of the summed individual response to the environment, influenced by the responses of neighbours (Parrish and Edelstein-Keshet, 1999). The scale of the swarm is also influential on the relative balance of behaviour and physical drivers on ultimate swarms shape (Folt and Burns, 1999). Over large scales (swarms of the order of 100–10 000 m length), behavioural processes (e.g. migration) are believed to combine with physical processes (turbulence, currents, and eddies) to generate heterogeneity in swarms shapes (Pinel-Alloul, 1995). Overall, smaller scales (0.1–10 m), individual behaviours, and responses can override physical processes (Zhou *et al.*, 1994).

Not all potential swarm shapes may be viable and the associated swarm shape parameters may be constrained within certain limits. Across different scales, the relationships between these parameters may follow geometric rules and some level of predictability in observed swarm shape may be apparent. Identifying these scaling rules have value in understanding the mechanisms of swarm formation (and break-up) since they can reveal patterns of assembly that are followed by individuals when joining (or leaving) an aggregation. Furthermore, the interaction between size and shape has wider implications to ecosystem function, particularly with regards a biomass dominant species such as Antarctic krill. The horizontal and vertical extent of swarms may influence their relative availability to different predator types, so differentially affecting foraging success (Croxall *et al.*, 1999;

Brierley and Cox, 2015). For instance, horizontally extensive swarms may benefit aerial predators whereas vertically extended swarms may be more exclusively available to diving predators. The biogeochemical role of swarms may also be affected by the relationship between size and shape, particularly in the ability of swarms to flux faecal pellet carbon to the ocean interior, which can be accelerated when swarms are vertically extensive (Tarling and Thorpe, 2017).

Krill are believed to aggregate active mainly through social interactions (Weber *et al.*, 1986). These interactions, in turn, are likely to be influenced by physiological factors, such as hunger and hypoxia, and external conditions, such as the presence of predators, food availability, and ambient temperature. Individual krill within swarms are able to behave collectively to their mutual benefit, for instance, in allowing them to retain favourable feeding locations (Tarling and Thorpe, 2014) or to obtain some physiological advantage (Ritz *et al.*, 2001; Swadling *et al.*, 2005). How these drivers translate to internal swarm structure is nevertheless complex and only limited insights have so far been gained. Kawaguchi *et al.* (2010) found that shoals of krill in captivity had nearest-neighbour distances of around 2–3 body lengths. Catton *et al* (2011) found krill to be aligned so that they were out of the downward wake of neighbours, as predicted from flow analysis on individuals by Wiese (1996).

At the whole swarm level, ultimate swarm shape may be further influenced by both the positive and negative consequences of group living. There is general consensus that swarming benefits its members by reducing predation risk through lowered predator encounter rate, collective vigilance, rapid information transfer, and predator confusion (Ritz *et al.*, 2011). Nevertheless, if predation was the only influence, then the optimal swarm shape should be spherical because this combines the smallest surface for any volume, minimizing both the risk of discovery and the number of individuals at the swarm edge (Brierley and Cox, 2010; Hemelrijk and Hildenbrandt, 2012). That this does not appear to be the case for the majority of swarms indicates that there are other antagonistic influences on swarm shape. One of the main costs of swarm membership is reduced feeding rates from exploitative and interference mechanisms (Folt, 1987). Furthermore, the reduced levels of diffusion may lead to waste products concentrating in the swarm interior to the point where they become toxic (Ritz *et al.*, 2011) and oxygen saturation drops to levels that are physiologically limiting (Johnson *et al.*, 1984). Such costs place a pressure on the swarm to disperse, so allowing greater diffusion and reducing the distance of individuals to the swarm edge. Ultimate swarm shape therefore reflects both the costs and the benefits of swarming.

A further influential factor on swarm shape is the scale of the swarm. Smaller swarms may not be under the same physical and biological influences as larger ones. For instance, levels of interference between individuals and diffusive flux to the swarm interior may be markedly different between small and large swarms. Conditions within the swarm must also remain within tolerable limits for individual swarm members if the swarm is to remain viable. These factors could mean that changes in swarm size are accompanied by changes in shape that follow certain allometric rules. This in turn will constrain the relationship between swarm shape parameters.

In this study, we examine a large dataset of krill swarms visualized acoustically during a scientific survey of the southwest Atlantic sector of the Southern Ocean. Our working hypothesis is that swarm shape, considered in terms of parameters such as area, perimeter, length, and vertical thickness, conforms to geometric scaling functions that limit their variability. We will test this hypothesis through considering scaling laws between various geometrical parameters and defining the ranges of their variability.

Our analysis considers data collected in two dimensions through what are three-dimensional objects, meaning that our insights into the true size and dimensions of any one individual swarm are limited. Nevertheless, the advantage of our dataset is that it consists of swarm cross-sections collected along preset transects, meaning that the direction passed through each individual swarm is random. Over a large number of swarms, the fact that each observation is random allows us to build up a picture of what patterns are common and what geometric relationships are statistically significant. We do not resolve the temporal evolution of swarm formation or break up of any one swarm but rather obtain an instantaneous picture of thousands of swarms within which we expect different states, or types, to exist. The insights we gain into geometric constraint on krill swarms are important in helping to identify the controlling influences on krill swarming behaviour. They are also useful when considering ecosystem structure, such as predator–prey dynamics and foraging on prey patches as well as the influence of different swarm formations on the flow of carbon through the system.

Methods

General survey details

A survey encompassing eight transects was carried out by the RRS *James Clark Ross* across the Scotia Sea between 9 January and 16 February 2003 (Figure 1a). The majority of transects were transited at 10 knots, although it was necessary to slow to around 5 knots in a small number of regions where conditions were icy. Acoustic data were collected using a SIMRAD EK60 echosounder connected to hull-mounted split-beam (38, 120, and 200 kHz) transducers. Only data from the 38 kHz and 120 kHz transducers were analysed to identify krill swarms to a maximum depth of 300 m. The beam angles, and hence sampling volumes, of both these frequencies were the same (7°) so allowing direct comparisons to be made for the purposes of swarm identification across most depths. An offset of the two sounders means that the beams were not overlapping at depths shallower than 25 m. Although this could lead to the misidentification of some krill swarms, we worked on the assumption that swarms of that shape, size, and backscattering strength were unlikely to be anything other than Antarctic krill in this part of the Southern Ocean. The surveys encompassed both open ocean and shelf regions, but all shelf data (data $<$ 100 km from nearest land) were excluded from the present analysis since swarms adopt very different formations in shelf environments and can be considered a special case worthy of separate investigation (Klevjer *et al.*, 2010). Data were collected continuously and subsequent analyses included both daytime and night-time periods.

Krill net sampling

A number of swarms were captured by net sampling to ground truth the acoustic records, principally for the purpose of establishing an acoustic target strength for krill. Krill swarms were located using the Simrad echosounder and then sampled with a rectangular midwater trawl (RMT8). The RMT8 was rigged with

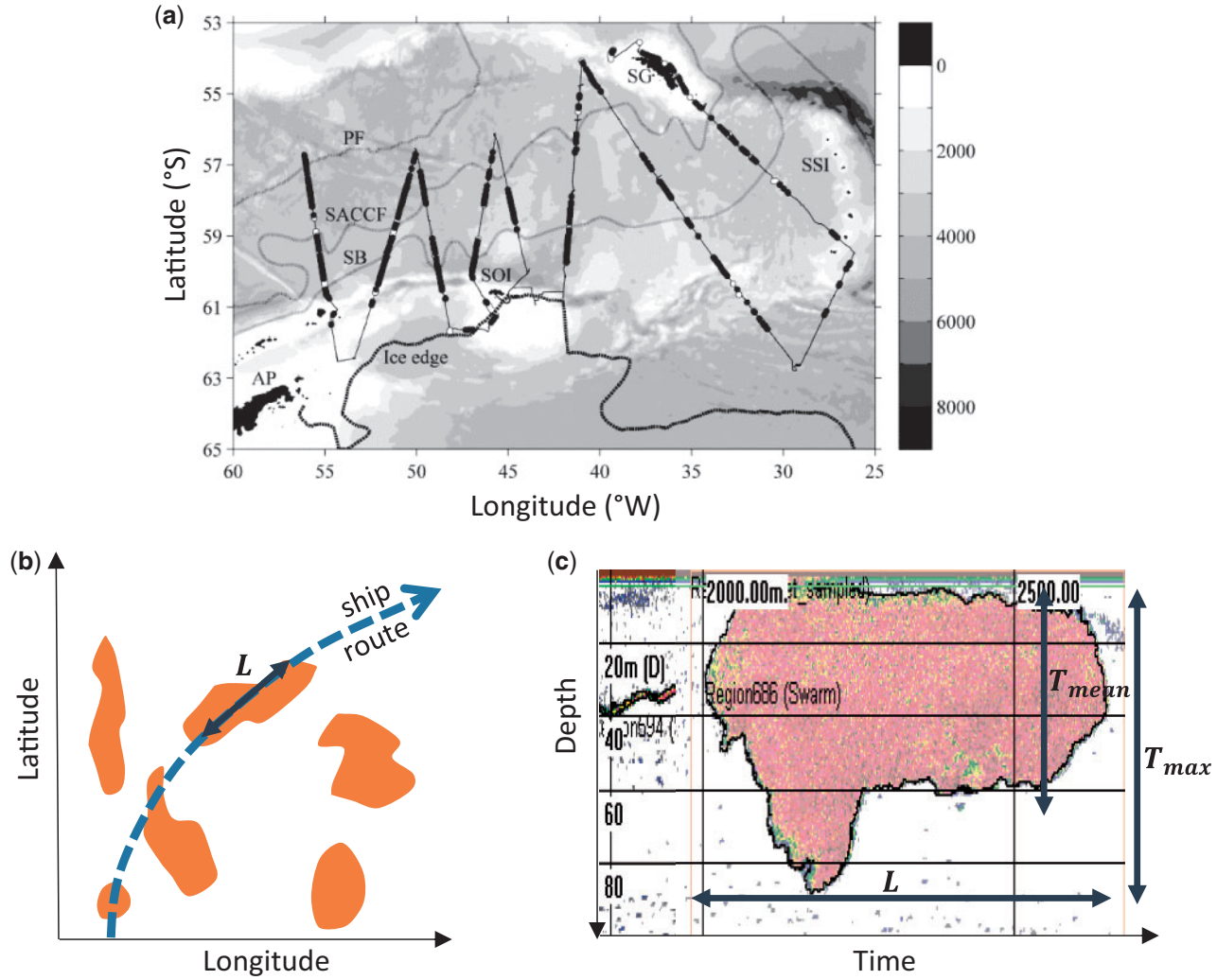

Figure 1. Swarms of Antarctic krill. (a) The ship route in the Atlantic sector of the Southern Ocean during the survey in 2003 highlighting in black circles the location of intercepted krill swarms. (b) A schematic representation of a ship route with respect to krill swarms (view from above). The ship route can intersect krill swarms at various angles. (c) Sampled echogram of a krill swarm obtained along the ship route (side view). The measured parameters: swarm length L is the maximal linear extent of the swarm along the ship route; maximal thickness T_{max} is the distance between the uppermost and lowermost parts of the swarm; area A is the filled area within the swarm; perimeter P is the total linear distance around the swarm edge. Additionally, we calculate the mean thickness as $T_{mean} = A/L$.

two remotely operated opening/closing nets, which had the capacity to sample separate swarms in close vicinity to one another. Krill sampling took place mostly during the hours of darkness. Full details of this analysis are provided in Tarling *et al.* (2009).

Acoustic data and processing

An acoustic system calibration was undertaken at Stromness Bay (54°9.44′S, 36°41.99′W) on 17 February 2003 using the standard sphere method (Foote *et al.*, 1987, 1990). Calibration was carried out with a 60-mm copper sphere for the 38 kHz transducers and a 23-mm copper sphere for the 120 kHz transducers (Tarling *et al.*, 2009).

Raw acoustic data from the 38 kHz and 120 kHz transducers were processed using Sonardata Echoview version 4.0 following the protocol of Hewitt *et al.* (2004) with the aim of excluding all backscatter not attributable to krill aggregations. Background noise was estimated and subtracted from the 38 and 120 kHz echograms (Watkins and Brierley, 1996), assuming that background noise levels follow a $20\log R + 2\alpha R$ relationship (where R is depth and α is the attenuation coefficient), which is then scaled to the minimum volume backscatter (S_v) in each layer during a transect before subtracting from the respective echograms. This method is particularly effective at decreasing the distortion with depth that would otherwise occur when identifying targets with a dB differencing approach (see below). Filters were applied to exclude the upper 13 m of the water column and depths below the detected bottom (where applicable) and other "bad data" resulting from interference or stormy weather. Smaller spikes were removed from the data by restricting the final swarm detection to those regions of the echogram where the 7 × 7 (pings × samples where the ping interval was 1.5 s and sample length, 0.1867 m) convolution-filtered data were above a threshold of –80 dB at 120 kHz. A threshold of –70 dB at 120 kHz was used in the subsequent swarm delineation, as advised by Lawson *et al.* (2008).

Krill swarm delineation

A swarm detection algorithm was applied to the processed 120-kHz echogram data using Sonardata Echoview version 4.0 "School detection module" (Sonardata Pty, Tasmania, Australia), which employs a SHAPES algorithm (Coetzee, 2000). This algorithm identifies data points that can be determined as "swarm candidates", which are groups of cells that meet minimum criteria for length and thickness. These individual swarm candidates are then linked together to form a larger swarm candidate if the horizontal and vertical distances between them are less than the specified maximum linking distances. After all linking has been carried out, swarms are recognized if the final swarm candidates are larger than the defined minimum total swarm length and thickness. With a ping interval of 1.5 s, and standard cruising speed of 10 knots, the minimum horizontal resolution was around 7.5 m. We set the minimum total swarm length to 15 m, which is double the minimum horizontal resolution. Transmit pulse duration was 1024 μs, giving an approximate pulse length of 1.5 m and a minimum vertical distance between two resolved targets of ∼75 cm. Minimum swarm candidate length and thickness were set to 10 m and 1 m, respectively. The maximum horizontal linking distance was set to 15 m, following Woodd-Walker *et al.* (2003), and the maximum vertical linking distance was set to 5 m. Swarms where the relative school length image compared to the beam width (Nb_i) was less than 1.5 were excluded from the dataset, following Diner (2001).

Swarms were detected from the 120 kHz echograms, and physical and acoustic descriptors for the detected swarm regions were exported from both 38 and 120 kHz data. These dimensions were corrected for known beam geometry according to the system of Diner (1998) within Sonardata Echoview 4.0. Detected swarms were interrogated to determine whether or not they were krill using the variable $\Delta S_{v120\text{-}38}$ identification technique (CCAMLR, 2005) following the steps outlined in Tarling *et al.* (2009), including the allocation of different krill total lengths to different survey regions in line with corresponding net catch results. This had a relatively minor influence on estimated krill target strength (TS) across the survey grid (Tarling *et al.*, 2018).

Swarm descriptors

Directions passed through swarms were random in that a swarm cross-section represents the transit across a swarm as the ship follows its preset route (Figure 1b). Once scaled according to distance travelled, we calculated a number of geometrical properties for each swarm cross-section: (i) P, the perimeter (m), (ii) A, the area of this section (m^2), (iii) L, the maximal horizontal extent (m), and (iv) T_{max}, maximal vertical extent (m). T_{max} represents the range between the uppermost and lowermost part of the swarm, which captures the fact that some parts of a swarm are located higher or lower in the water column than others. An alternative measure is the mean thickness averaged along swarm length, which can be defined as (v) $T_{mean} = A/L$. This parameter defines the average distance between the upper and lower borders of a swarm and is always smaller than T_{max}. For convenience, we also denote the logarithm of swarm thickness as $\tau = \log_{10} T$.

Numerical analysis

We investigated relationships between swarm descriptors through regression-based analyses. All regressions were carried out in the logarithmic domain with the Matlab routine `fitln` using the relationship $\log y = b + k\log x$. In most cases, the results were later converted into a more convenient power law form, $y = 10^b x^k$.

Results

Scaling of length and thickness

There was a wide range of swarms sizes detected in the survey, with swarm length varying from 1 to 10 000 m, maximal thickness from 1 to 100 m, and the average thickness from 0.3 to 10 m. To give an insight into swarm size distributions, consider the bivariate histograms showing the distribution of swarms in $(L,\ T_{max})$ coordinates and $(L,\ T_{mean})$ coordinates (Figure 2a and b).

The distribution of swarm thicknesses shifts toward greater values as swarm length increases. To take into account the dependence of the distribution parameters on swarm length, we fit them for each length bin separately. The histogram of logarithmic thickness (both maximal, T_{max}, and average, T_{mean}) in each length bin can be closely approximated by a normal distribution truncated at the minimum detection limit for swarm thickness of 1.27m (Supplementary Figure S1)

$$P_L(\tau) \propto \exp\left(-\frac{(\tau-\tau^*(L))^2}{2\sigma^2(L)}\right)\theta(\tau-\tau_{min}) \qquad (1)$$

where both the mean $\tau^*(L)$ and variance $\sigma^2(L)$ depend on swarm length, $\theta(\tau-\tau_{min})$ is the Heaviside function, and τ_{min} is the logarithmic thickness of the thinnest detected swarm (see Supplementary Appendix A for the fitting details). A Shapiro–Wilk test confirmed the normality of these distributions at the significance level $\alpha = 0.01$ for swarms longer than $L > 30$m. The obtained maximal likelihood estimates for $\tau^*(L)$ and $\sigma(L)$ with error bars indicating 95% confidence interval are shown in Figure 2.

The most likely logarithmic maximal thickness τ^*_{max} (Figure 2a) and average thickness τ^*_{mean} (Figure 2b) monotonically increase with swarm length. While τ^*_{max} increases proportionally to the logarithm of length over the entire range, the average thickness τ^*_{mean} remains approximately constant (around 1 m) for swarms shorter than 40 m and begins to increase with L for longer swarms. The linear regression analysis (Table 1) shows that the most likely maximal thickness increases as $\tau^*_{max}(L) = -0.62 + 0.69\log_{10} L$ (Figure 2a) and its standard deviation decreases as $\sigma(L) = 0.51 - 0.11\log_{10} L$ (Figure 2a). For the average thickness, we obtain $\tau^*_{mean} = 0.058$ ($T^*_{mean} = 1.14$m) for $L < 40$ and $\tau^*_{mean} = 0.69 + 0.47\log_{10} L$ for $L \geq 40$m and $\sigma = 0.39 - 0.05\log_{10} L$. Thus, both maximal and average thickness increase slower than swarm length. For instance, for $L \geq 40$m, the average thickness increases approximately as a square root of length, $T^*_{mean} = 4.9L^{0.47} \approx 4.9\sqrt{L}$, meaning that a two order of magnitude increase in swarm length (e.g. from 40 to 4000 m) leads only to approximately one order of magnitude increase in the average thickness (from 27 to 240 m for the given example).

Scaling of swarms in the vertical realm

We obtain an additional perspective on the scaling of swarm shape from the distribution of T_{max}/T_{mean}, which is the relative vertical maximum swarm extent with respect to mean thickness. This parameter can be interpreted as swarm flatness, as it increases when the vertical swarm variation increases without increasing the mean thickness, and it approaches 1 for an absolutely flat swarm with no variation along the vertical axis. Swarm

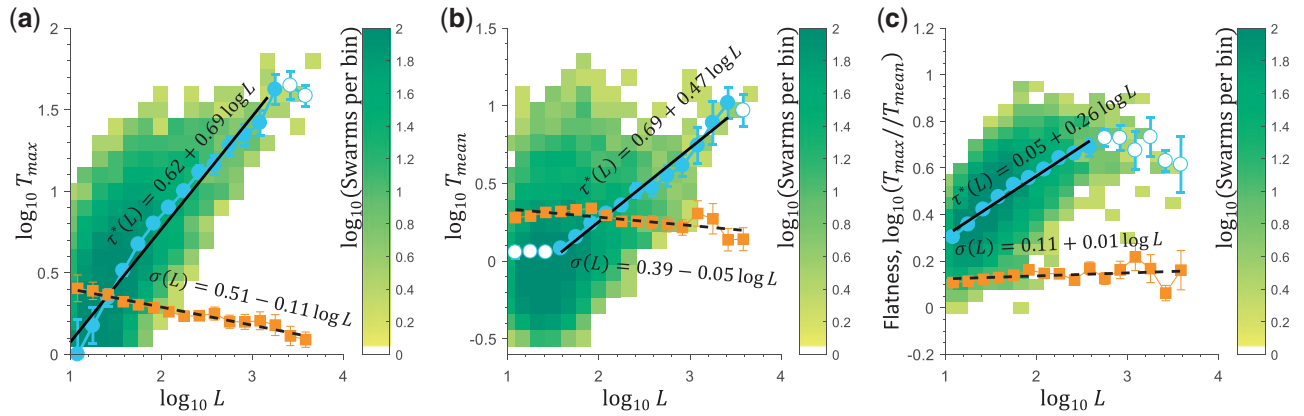

Figure 2. Length and thickness distribution of krill swarms in the south-west Atlantic sector. Bivariate swarm distribution (colour coded) of logarithms of swarm length vs. (a) maximal thickness, T_{max}, (b) mean thickness, T_{mean}, and (c) flatness, T_{max}/T_{mean}. The grid is logarithmically binned with step 1/6 for $\log_{10} L$ and 0.1 for vertical axes. Within each length class (vertical grid columns), the distribution closely follows a normal distribution truncated at the detection limit (see Supplementary Figure S1 for some examples). The maximal likelihood estimates for the parameters of the distribution: most likely logarithmic thickness $\tau^*(L)$ (open and closed blue circles) and variance $\sigma(L)$ (orange circles), the error bars show standard error. The linear regression (excluding outlier points marked as blue open circles) of the mean values (black solid line) and the variance (black dashed line). See Table 1 for the regression parameters.

Table 1. Linear regression parameters for $\tau^* = b + k\log_{10} L$ and $\sigma(L) = b + k\log_{10} L$ for Figure 2.

	$b \pm$stand. err	$k \pm$stand. err	R^2_{adj}
Figure 2a			
$\tau^*_{max}(L)$	-0.62 ± 0.07	0.69 ± 0.03	0.98
$\sigma(L)$	0.51 ± 0.02	-0.112 ± 0.007	0.95
Figure 2b			
$\tau^*_{mean}(L)$	-0.69 ± 0.07	0.47 ± 0.03	0.97
$\sigma(L)$	0.39 ± 0.03	-0.05 ± 0.01	0.47
Figure 2c			
$\tau^*(L)$	0.05 ± 0.02	0.26 ± 0.01	0.98
$\sigma(L)$	0.11 ± 0.03	0.01 ± 0.01	0.02

flatness first increases with length from 2 for $L = 10$m to 5 for $L \approx 400$m and then stays at a constant level or even decreases for extremely long swarms with the average value of $\langle T_{max}/T_{mean} \rangle \approx 4.8$ in this range (Figure 2c).

The swarm aspect ratio, T_{max}/L, decreases with swarm length (Figure 3a). Aspect ratio is greatest in the smallest swarms but declines dramatically as swarms increase in length. Using the dependence of the most likely maximal thickness on the length to estimate the aspect ratio we obtain:

$$\frac{T^*_{max}}{L} = 0.26 L^{-0.32} \tag{2}$$

i.e. the aspect ratio decreases approximately inversely proportional to the cubic root of L. As shown in Figure 3a, this equation provides a good approximation to the linear regression through the data points. For example, although 10 m long swarms exhibit an aspect ratio of around 1 m of thickness per 5 m for length, 1000 m long swarms have proportions of 1 m of thickness per 30 m or more of length.

Scaling of perimeter to area

Swarm area and perimeter can be approximated by a power function of length and maximal thickness (Figure 4). The swarm area scales as $A = 0.8 L^{0.77} T_{max}$ and perimeter as $P = 3.5 L^{0.86} T^{0.48}_{max}$. Both functions describe 95% of the variance in swarm area and perimeter.

The scaling of swarm area allows us to make some conclusions concerning the scaling of the average swarm thickness. Using the scaling expression for area, we can calculate the average thickness as $T_{mean} = A/L = 0.8\ T_{max} L^{-0.23}$ m. Thus, on average, the mean swarm thickness is smaller than the maximal thickness T_{max} by the factor $0.8 L^{-0.23}$.

The area-specific length of perimeter, surface roughness $R = P/A$ on average equals 3.17 m^{-1}. Using the scaling laws for area and perimeter, we find:

$$R = \frac{P}{A} = 4.36\ L^{0.09} T^{-0.52}_{max}\ \text{m}^{-1} \tag{3}$$

Thus, surface roughness has an extremely weak dependence on length and mainly depends on swarm maximal thickness. Indeed, the factor $L^{0.09}$ changes from 1 for $L = 1$m to 2.29 for $L = 10\ 000$m. Thus, the main variations in the surface roughness are related to the changes in thickness. Using median value $L_{median} = 41$m, we obtain the following approximate equation for swarm roughness:

$$R_{appox} = 4.36\ L^{0.09}_{median} T^{-0.52}_{max} = 6.16 T^{-0.52}_{max}\ \text{m}^{-1} \tag{4}$$

Hence, surface roughness is approximately inversely proportional to the square root of swarm thickness. Equation (4) closely approximates a linear regression of data points (Figure 3b).

It is not surprising that surface roughness decreases with swarm size because perimeter typically grows slower than area with increasing size. It is more informative, therefore, to compare surface roughness with roughness of a smooth geometrical figure with the same linear dimensions. For this purpose, we calculate surface roughness of ellipses with the same length and thickness (Figure 3b). As shown in Supplementary Appendix B, and confirmed by linear regression of the data, the roughness of an ellipse decreases approximately as $1/T_{max}$, which is much faster than the

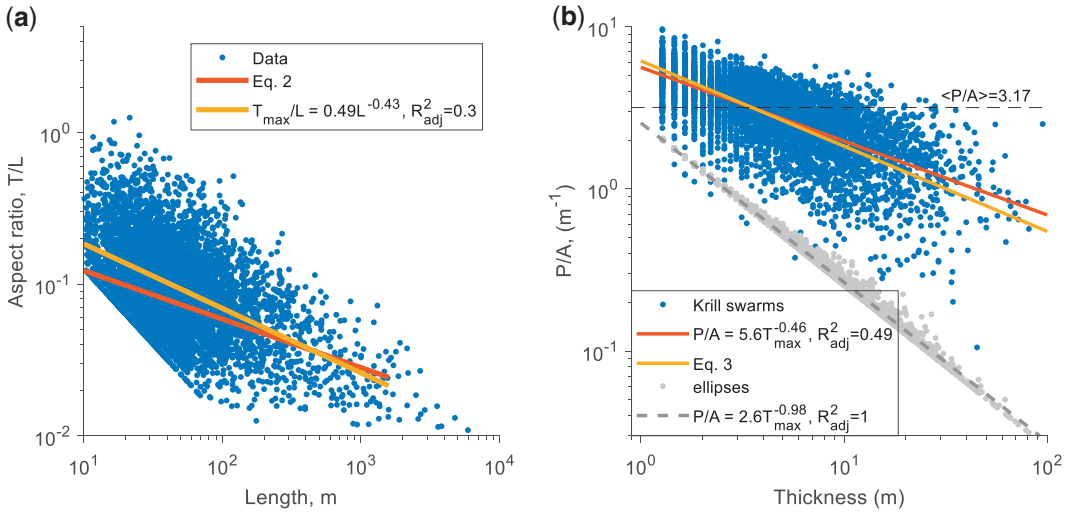

Figure 3. Scaling of swarm aspect ratio and surface roughness. (a) Aspect ratio (thickness/length) of krill swarms as a function of length (blue/darker dots), linear regression of data (yellow/lighter line) in comparison with an approximation provided by Equation (2) (red/darker line). (b) Surface roughness (perimeter/area) of krill swarms as a function of swarm thickness (blue/darker dots) compared to the surface roughness of ellipses with the same linear dimensions (grey/lighter dots) with the average level of 3.17 m^{-1} (black dashed line). Linear regression of surface roughness of krill swarms (red/darker line) in comparison with an approximation provided by Equation (3) (yellow/lighter line). Linear regression of the surface roughness of ellipses (grey dashed line).

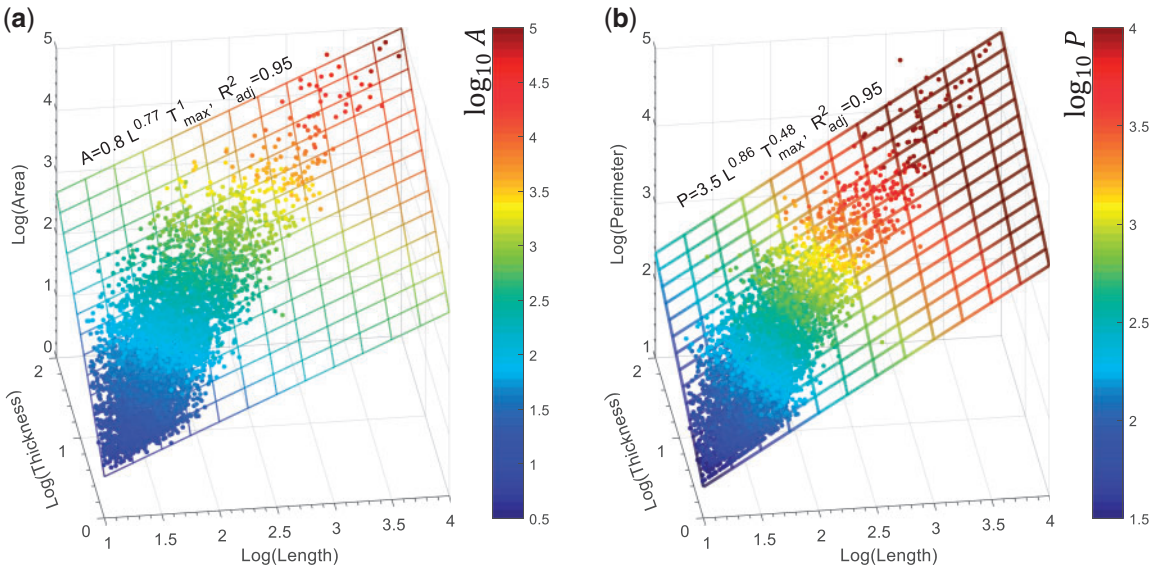

Figure 4. Scaling rules for swarm area (a) and perimeter (b). Swarm area and perimeters (dots) fitted with planes (grid lines) in log-log space. The colour coding of the grid lines on the planes and data points matches the vertical coordinates ($\log_{10} A$ and $\log_{10} P$) to highlight the closeness of data points and fitted planes. Both fittings explain 95% of variance in the data.

decrease of surface roughness we observe in krill swarms ($1/T_{max}^{0.46}$). Increasing swarm size appears to be accompanied by the appearance of new cavities and indentations in the swarm structure which leads to an increase in the perimeter. As a result, the perimeter of thick swarms can be up to 10 times greater than the perimeter of an ellipse with the same linear dimensions.

Swarm categorizations

To address the hypothesis that swarm size constrains swarm shapes to certain types, we compare the area and perimeter of swarms with that of dimensionally equivalent ellipses. We denote the relative elongation in swarm perimeter with respect to ellipse perimeter as $\varepsilon_P = P/P_{ell}$ and ratio of swarm to ellipse area as $\varepsilon_A = A/A_{ell}$. For most swarms, ε_P is greater than 1 and ε_A is less than 1. Only in extremely rare situations, e.g. when the swarm shape approaches, for instance, a rectangular or rhombus, are these rules are violated (see frequencies of swarms with different values of ε_P and ε_A in Figure 5b). The greatest concentration of swarms is around the median values $\varepsilon_P^* = 1.9$ and $\varepsilon_A^* = 0.4$. Thus the most frequent swarms are approximately 2 times greater in perimeter and 2 times smaller in area than the corresponding ellipse.

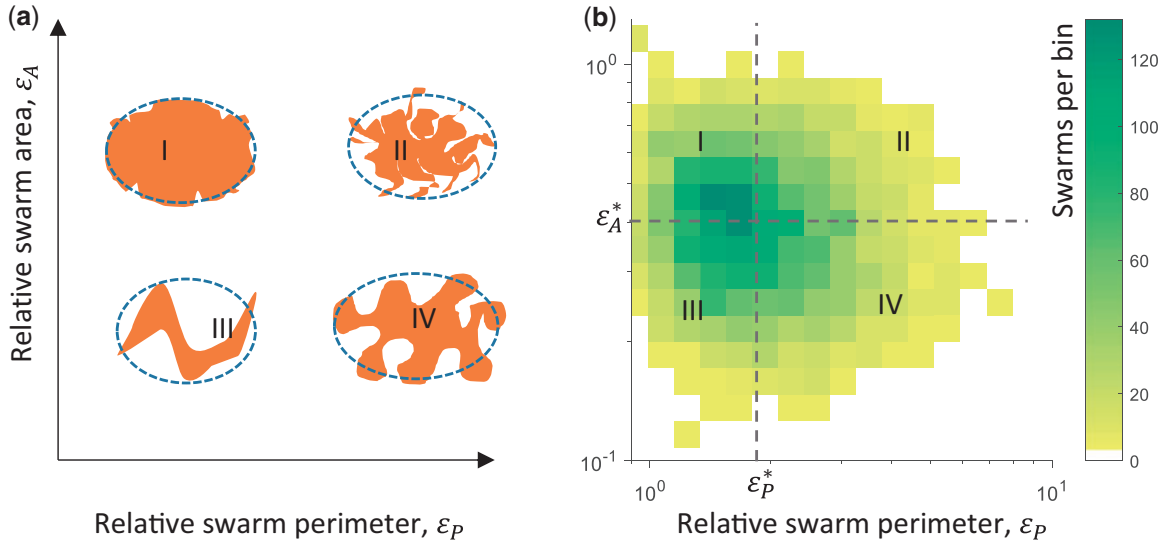

Figure 5. Classification of krill swarms. (a) A schematic representation of different classes of swarm shapes. The shape of swarms (orange) is compared to an ellipse (blue dashed line) with the same linear dimensions. As coordinates, we use the relative swarm area, ε_A, and relative perimeter, ε_P, with respect to the area and perimeter of the corresponding ellipse. We introduce the following classes (I) *Ellipsoidal* swarms: perimeter and area are close to the perimeter and area of an ellipse. (II) *Filamentous* swarms: the area approximately equals the ellipse area, but the perimeter is larger. (III) *Needle-like* swarms: the perimeter is approximately equal the ellipse perimeter, but the area is smaller than the ellipse area. (IV) *Indented* swarms. The area is smaller than the area of an ellipse, but the perimeter is greater than the ellipse perimeter. (b) A bivariate plot of swarm distribution as a function of relative swarm area, ε_A, and relative perimeter, ε_P. The number of swarms as a function of the relative area and perimeter (logarithmically binned). The border separates different swarm classes (dashed lines).

However, these swarms represent less than 10% of the total swarm number because most of the swarms are distributed within the peripheral areas of the plot.

Using the median values as thresholds, we split swarms into the following four equally abundant classes (Figure 5a) with distinctly different geometrical properties. (I) *Ellipsoidal* swarms: perimeter and area are close to the perimeter and area of an ellipse—these swarms are the most compact and their shape approaches that of an ellipse. (II) *Filamentous* swarms: the area approximately equals the area of an ellipse, but the perimeter is larger due to filaments and fjords in the swarm structure—these swarms are still compact apart from at the edges. (III) *Needle-like* swarms: the perimeter approximately equals the ellipse perimeter, but the area is smaller—these swarms are thin and elongated with a small number of cavities. (IV) *Indented* swarms: the area is smaller than the area of the corresponding ellipse, but the perimeter is greater—these swarms have the largest perimeter and smallest area, and therefore, the highest surface roughness for given linear dimensions.

How does the swarm class depend on swarm linear dimensions? To answer this question, consider the change in ε_P and ε_A with swarm maximal thickness and length (Figure 6). Although the pattern is relatively noisy, we observe clear gradients with the perimeter ratio ε_P increasing mainly with swarm thickness and area ratio ε_A decreasing with swarm length. The dashed lines show the isolines where the averaged values of ε_P and ε_A equal the threshold levels ε_P^* and ε_A^* (see also Supplementary Figure S2). Superpositioning of the threshold levels gives us the swarm class partitioning in (L, T_{max}) axes and shows what types and sizes of swarms are geometrically compatible (Figure 6c).

Our comparison of the swarm and ellipse surface roughness (Figure 3b) shows that roughness of geometrical shapes typically decreases with shape size. This fact hampers a direct comparison of the roughness of differently sized swarms and produces a false sense that larger swarms should be smoother whilst, in reality, larger swarms possess a more complex perimeter structure. Generalizing our approach further, we define the relative swarm roughness as $\rho = R_{swarm}/R_{ellipse}$, where $R_{ellipse}$ is the roughness of an ellipse with the same linear dimensions. It is easy to check that the relative roughness can also be expressed in terms of the relative perimeter and area as $\rho = \varepsilon_P/\varepsilon_A$. Combining the estimations of the average swarm roughness, Equation (3), with ellipse roughness (Supplementary Appendix B) we find that the average relative roughness scales as

$$\rho = 1.72\ L^{0.09}\ T_{max}^{0.48} \tag{5}$$

Thus, the relative surface roughness depends mainly on the changes in the vertical swarm extent, increasing approximately as the square root of T_{max}, and is nearly independent of the swarm length.

Discussion

Through examining a large dataset of acoustically visualized krill swarms in the southwest Atlantic sector of the Southern Ocean, we identified that the shapes adopted by swarms varied according to their size. We uphold our working hypothesis that the influence of geometric constraints is strong on relationships between swarm parameters such as area, perimeter, length, vertical thickness, and swarm shape. Not all swarm shapes appeared possible at all scales, and whereas swarms could be smooth and vertically thick at smaller scales, larger scale swarms either exhibited relative thinning or increased number of indentations and filaments. We discuss further the nature of these geometric relationships and

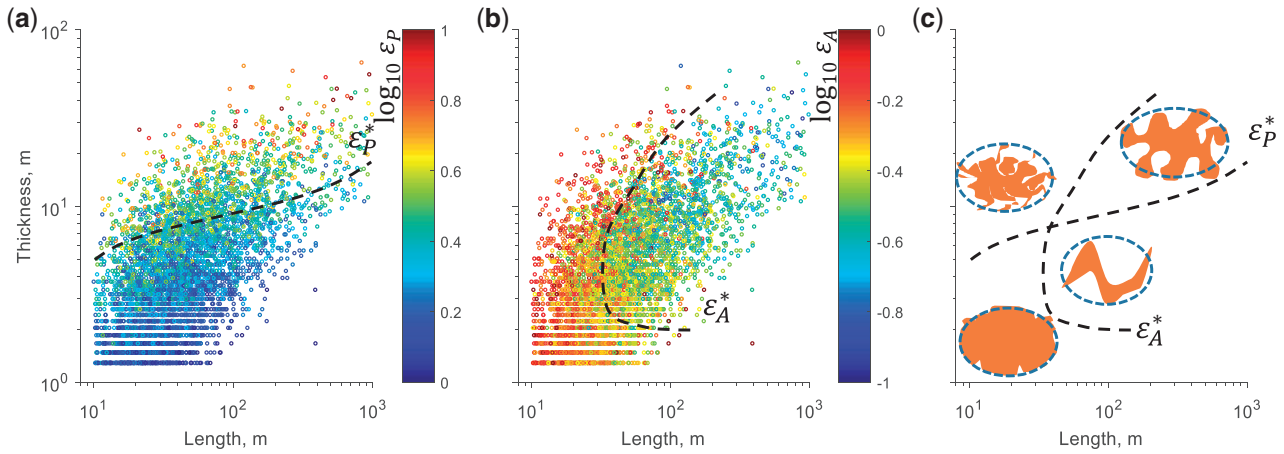

Figure 6. Swarm classification as a function of length and thickness. (a) Swarm relative perimeter ε_P (colour coded) as a function of swarm length and maximal thickness. (b) The same but for swarm relative area ε_A. (c) Location of the swarm classes in $(L,\ T_{max})$ coordinates. Threshold levels ε^*_P and ε^*_A (black dashed lines).

consider potential environmental and physiological factors that may influence them.

Scaling of length and thickness

We found that swarms were more likely to lengthen than to increase in vertical thickness as the scale of the swarm increases. The effect is most exaggerated in the largest swarms because thickness grows approximately as the square root of length and a two order of magnitude increase in length (e.g. from 40 to 4000 m) results in only a one order of magnitude increase in thickness (from 27 to 240 m in the given example). From the perspective of swarm shape, therefore, an increase in swarm size is mostly observed as an increase in length and not thickness. This is also observed when deriving a scaling of the aspect ratio (T/L) which we found to decrease as the power of swarm length. Whereas 10 m long swarms exhibit an aspect ratio of around 0.2 (1 m thickness per 5 m length), 1000 m long swarms have a ratio of 0.03 (1 m of thickness per 30 m or more of length), indicating that increases in length are not accompanied by proportional increases in thickness.

Aspect ratio was also considered in Antarctic krill swarms found in Crystal Sound and Marguerite Bay as well as Laubeuf fjord by Zhou and Dorland (2004). They found that aspect ratio in the Crystal Sound and Marguerite Bay population differed considerably from that in the Laubeuf Sound population, with the former tending toward a ratio of 0.05 and the latter, 0.01–0.03. This was attributed to lateral stretching by the greater levels of advection in Laubeuf Sound. Furthermore, swarms in Laubeuf Sound were longer than those in Crystal Sound and Marguerite Bay, which would also contribute to the general decrease in aspect ratio, as we found in the present study.

The tendency for swarms to lengthen but not thicken vertically with increasing swarm size may also be influenced by individual swimming behaviour and inter-individual relationships. Antarctic krill swims through the metachronal beating of its abdominal appendages (pleopods) which, unlike fish, does not involve any undulation of the body. This means that they do not require as much lateral space on either side to swim without interference. Packing concentrations of krill in Scuba and laboratory observations are notably high, with minimal nearest-neighbour distances between 1.5 and 3 body lengths being reported (O'Brien, 1989; Kawaguchi *et al.*, 2010; Catton *et al.*, 2011). Collectively, krill generate considerable downdrafts (Kils, 1981; Catton *et al.*, 2011; Tarling and Thorpe, 2017), which are necessary to overcome their negative buoyancy (Kils, 1981). From an individual perspective, it is less energetically expensive for a krill to join others through swimming in front of, behind, or to the side of existing swarm members rather than to join from above or below. In terms of small aggregations, avoidance of any collective downdrafts below the swarm would also make joining another swarm laterally less costly energetically than from beneath. Scaled up to the level of the swarm therefore, adding to the length rather than the vertical thickness of a swarm appears to be a more energetically efficient strategy, which is consistent with our observations.

Scaling of swarms in the vertical realm

We distinguished between two measures of vertical swarm thickness, T_{max}, which represents the maximum distance between the upper and lower extremities of a swarm, and T_{mean}, which is the mean vertical thickness across the entire length of a swarm. We found that the average T_{max} monotonically increased as a power of swarm length, faster than the average T_{mean}, which stayed approximately constant at around 1 m for swarms shorter than 50 m and only then began to increase. The ratio of T_{max} to T_{mean} increased for swarms shorter than 400 m length and levelled off at around 5 for longer swarms. The fact that T_{mean} always remained about 1/5th of T_{max} in larger swarms indicates that external swarm shape remains relatively conservative with regards the relationship between vertical extremities and the main body of the swarm.

Both biological and physical factors may limit the T_{mean} and T_{max} of large swarms. Biologically, the euphotic zones reaches it maximum depth between 50 and 80 m in the Scotia Sea (Korb *et al.*, 2012), such that primary production is unlikely to occur below such depths. Thus, deeper than 100 m, krill may have limited possibilities to feed on fresh phytoplankton. Nevertheless, Tarling and Thorpe (2017) demonstrated that individuals are

likely to move vertically within the body of a swarm and rotate through the main phytoplankton layers as they repeatedly feed and sink. This behaviour has also been observed in mysids (Buskey, 1998). The behaviour allows individuals within vertically thick swarms access to the food layers, at least for a period of time. Maximum vertical thickness may accordingly represent the distance over which individuals sink after feeding before returning to the upper layers to feed once again. This sinking behaviour may also influence the relatively fixed relationship between T_{max} and T_{mean} in larger swarms.

The structure of the water column may also present vertical limits to swarm coherence. In summer, the upper mixed layer reaches a maximum depth of around 100 m in the Scotia Sea (Venables *et al.*, 2012), below which is colder Winter Water (Gordon *et al.*, 1977). The pycnocline at the bottom of the mixed layer may be a physical barrier to further vertical expansion of a swarm. Furthermore, the strength and direction of currents in the upper mixed layer and the underlying Winter Water may differ (Murphy *et al.*, 2004), potentially presenting a shear that may challenge the ability of deeper individuals to remain with the rest of the swarm.

Scaling of perimeter to area

The perimeter of an object will always decrease relative to its area if the object increases in size while retaining the same shape. We calculated this effect for ellipses with the same dimensions and showed that if $L \gg T_{max}$ (which is a valid assumption for most swarms), the perimeter-to-area ratio (surface roughness) should decrease as $1/T_{max}$ (see Supplementary Appendix B). However, for krill swarms with increasing T_{max}, we found that surface roughness in krill swarms decreases less steeply and can be approximated as the inverse square root of T_{max}. This means that the perimeter of krill swarms grows with swarm length faster than compared to the perimeter of an ellipse. To highlight this effect, we introduced the relative roughness parameter, ρ, as the ratio of swarm roughness to ellipse roughness. This value increases approximately as the square root of the swarm maximal thickness and has only a weak positive dependence on swarm length. This measure of swarm roughness is more consistent with an intuitive expectation of what should happen when two swarms merge. For instance, joining two similar swarms in the same horizontal layer may double the swarm length but should have only a weak effect on the swarm thickness and perimeter structure. This is reflected in the weak dependence of the relative roughness on swarm length. In contrast, a vertical merging of two swarms can double the swarm thickness and lead to a more complex and rougher perimeter structure with a larger number of cavities and filaments. We observe an increase of the relative swarm roughness with increasing thickness.

In their analysis of the three-dimensional structure of Antarctic krill swarms using a multibeam sonar in inshore locations, Brierley and Cox (2010) found that swarm size and packing density varied greatly but surface area: volume (3D surface roughness) ratios were distributed around a fixed value of 3.3 m^{-1}. This is not entirely consistent with our own observations of surface roughness, albeit with our two-dimensional rather than three-dimensional perspective, since we found that surface roughness decreases with increasing swarm size. Nevertheless, we agree with the findings of Brierley and Cox (2010) in two regards, first in the mean perimeter: area ratio being approximately the same as the surface area: volume ratio (3.2 m^{-1} vs. 3.3 m^{-1}, respectively) and, second, that with increasing swarm size, surface area (or perimeter in the present case) increased less than area of an equivalent isometrically scaled object. The three-dimensional visualizations provided by Brierley and Cox (2010) provides an unrivalled insight into swarm structure although their krill surveys were more spatially limited and likely encountered a comparatively smaller spectrum of swarm types than those considered in the present study. In the future, it would be instructive to carry out intercomparisons of two- and three-dimensional visualizations from data collected simultaneously to consider how respective geometric relationships (e.g. surface area to volume vs. perimeter to area) relate to each other. The wider use of lower-frequency sonar would be particularly useful in this regard (Makris *et al.*, 2006).

Further influences on geometric relationships

Variance around geometric relationships likely results from both internal and external factors. Internally, packing concentrations will influence the external smoothness of swarms. Tighter packing will be generated from the polarization of individuals, which potentially is a response to predator avoidance or a product of directional horizontal migrations (Hamner and Hamner, 2000). Predator avoidance behaviour may be particularly acute in shelf regions close to higher predator colonies which may be responsible for the considerably different swarming patterns observed in such regions (Klevjer *et al.*, 2010). Looser packing is generated from more individualistic behaviour, as would result from filter feeding when encountering a patch of phytoplankton (Kawaguchi *et al.*, 2010). Externally, day–night differences are likely to be a major source of variance. Tarling *et al.* (2018) found that levels of dissimilarity between certain swarm parameters altered according to time of day with, for instance, area and perimeter exhibiting a significant linkage in similarity during the daytime, but no linkage during dusk and night time. The authors concluded that swarm parameters were more variable than depth over the diel cycle. Distinguishing the individual contributions of these factors to variance in geometric relationships is nevertheless far from straightforward given that there will also be inter-relationships between the factors themselves, e.g. individualistic behaviour from feeding is more likely to occur during dusk and night time.

Swarm categorizations

Based on the relationship between perimeter and area, we classified krill swarms into four shape types, which we termed *Ellipsoidal*, *Filamentous*, *Needle-like*, and *Indented*. Certain features of the different swarm types suggest the influence of different behaviours. For instance, swarm types with lower than average perimeters (*Ellipsoidal* and *Needle-like*) are most compact and retain a relatively smooth periphery, which may reflect that individuals within these swarms are tightly aggregated. At a behavioural level, this could be generated through krill being in a phase of active horizontal migration, where nearest-neighbour distances are reduced and relative positions become polarized in order to gain maximal hydrodynamic benefit (Wiese, 1996; Catton *et al.*, 2011). Reduction of the perimeter may also be a response to predators such that the largest possible proportion of individuals occupy internal sheltered positions away from the edge (Brierley and Cox, 2010).

Indented swarms have above average perimeter but below average area and are more amorphous in shape. The shape likely

reflects that packing concentrations are not uniformly high, resulting in large indents in the external shape of swarms and possibly even vacuoles within the body of the swarm. Such features have also been identified in fish schools (Fréon *et al.*, 1992; Rieucau *et al.*, 2015), taken to indicate that individuals were exhibiting more individualistic or exploratory behaviour in low stress situations with greater inter-individual distances and lower polarization. This would be consistent with krill swarms that are exploiting patches of food, particularly in terms of using their feeding baskets to filter food particles where greater inter-individual distances would be required (Hamner, 1984; O'Brien, 1988).

Filamentous swarms may also be a product of more individualistic behaviour although their above average areas indicate that a larger proportion of individuals are some distance away from the swarm nucleus. This suggest some heterogeneity in the tendencies of individuals with only local groups reaching out from the swarm edge to form filaments (Parrish and Edelstein-Keshet, 1999). These local groups may have different physiological states to the larger majority, which may require differing levels of feeding. For instance, in Northern krill, Tarling (2003) found that females, to meet their greater energetic demand, were prepared to take greater levels of risk and feed in more dangerous but more productive layers compared to males and sub-adults. Individuals about to moult or mate may also displace themselves from the body of the swarm to avoid cannablism of themselves or their offspring, respectively (Tarling *et al.*, 1999). The filaments may otherwise reflect a stage prior to the break-up of a swarm, akin to the "stretch and tear" phases of fish schools described by Fréon *et al.* (1992).

Besides different behavioural constraints, swarm shape type is also constrained by swarm size. Thin swarms are mostly either *Ellipsoidal* (when short) or *Needle-like* (when long). In contrast, most thick swarms are characterized by a complex perimeter and are either *Filamentous* (when short) or *Indented* (when long). This relationship occurs because the relative swarm area and perimeter strongly depend on swarm thickness and length. An increase of swarm thickness increases mainly the relative perimeter ε_P but not relative area ε_A, which can be associated with an increased amount of filaments and indentations at the swarm edge. In contrast, increasing swarm length reduces swarm relative area but not perimeter. The area of short swarms, independently of their thickness, is close to the area of an ellipse with the same dimensions but the area of long swarms tends to be nearly one order of magnitude smaller than the area of an ellipse. Thus, indentation and relative thinning appear to be a necessary feature for long swarms to remain coherent.

Influence of swarm shape and size on ecosystem function

Knowledge of the spectrum of shapes and sizes of swarms have a utility to considering how ecosystems are structured. For Southern Ocean ecosystems in particular, interactions between higher predators and their krill prey has a dominating influence on how the system functions (Murphy *et al.*, 2007). Different predators have widely varying methods of foraging. The ways in which they exploit food patches are an important aspect of their life cycle, shaping their response to varying levels of prey availability (Croxall *et al.*, 1999). Here we illustrate that horizontally extensive krill swarms are unlikely to be also vertically extensive. This may therefore differentially favour aerial foragers who have the ability to locate rare but large patches and exploit them from surface layers (Grünbaum and Veit, 2003). Diving predators, in contrast, may benefit more from exploiting smaller swarms, which are more likely to be thicker relative to their length and more exclusively available to predators that can forage deeper for their prey (Croxall *et al.*, 1985). Our parameterizations can be used to recreate prey fields in models to test these hypotheses (e.g. Cresswell *et al.*, 2007).

Antarctic krill are also increasingly recognized as a major conduit for carbon export to the ocean interior through large-scale deposition of sinking faecal pellets (Belcher *et al.*, 2017). Not all swarms may be equally as efficient in this process, and swarm shape may be a major determinant of export efficiency. Vertically extensive swarms are likely to release faecal pellets toward the bottom of the mixed layer (Tarling and Thorpe, 2017), while pellets released by long and thin swarms may have further to travel before reaching the ocean interior, increasing their chance of interception and remineralization by coprophagous species. We provide a means of accounting for the types and characteristics of different swarm shapes that may assist in the determination of carbon export efficiency by krill.

Concluding remarks

We identified rules that govern the comparative external dimensions of open ocean krill swarms. We identify clear geometric relationships between swarm parameters and uphold the hypothesis that swarm shape is bound by geometric functions across scales. These rules are likely to reflect a combination of physical and biological influences that are external to the swarm and behavioural interactions between individuals within the swarm itself. As swarms increase in size, they tend to lengthen horizontally far more than thicken vertically and this likely reflects both biological and physical constraints placed on swarm dimensions. We also identified characteristic relationships between the perimeter and area of swarms, variance in which may reflect different stages in the time course of swarms, particularly phases of feeding and horizontal migration. Certain shapes may also indicate heterogeneity between swarm members with regards to physiological state. Although the shapes of krill swarms are highly variable, we demonstrate that there is some predictability in their dimensions. These findings will have utility both to considering the size and shape of food patches for krill predators and in accounting for the biogeochemical role of different swarms types.

Supplementary data

Supplementary material is available at the *ICESJMS* online version of the manuscript.

Acknowledgements

We thank the contribution of the two anonymous referees whose insights and suggestions greatly improved this manuscript. We are grateful to the crew and scientists aboard the RRS James Clark Ross during the cruise JR82 for their assistance in collecting material. We also thank D. Bone for assembling and maintaining the net gear and N. Cunningham for organizing and retrieving data. S. Fielding and T. Klevjer assisted in the acoustic identification and visualization of krill swarms, as reported in previously published works. ABR acknowledges the Lower Saxony Ministry for Science and Culture, project POSER. GT acknowledges COMICS (UK Natural Environment Research Council, Large grant NE/

M020762/1) in supporting the write up of this manuscript. The work was carried out as part of the Ecosystems programme at the British Antarctic Survey and Natural Environment Research Council.

References

Belcher, A., Tarling, G., Manno, C., Atkinson, A., Ward, P., Skaret, G., Fielding, S., *et al.* 2017. The potential role of Antarctic krill faecal pellets in efficient carbon export at the marginal ice zone of the South Orkney Islands in spring. Polar Biology, 40: 2001–2013.

Brierley, A. S., and Cox, M. J. 2010. Shapes of krill swarms and fish schools emerge as aggregation members avoid predators and access oxygen. Current Biology, 20: 1758–1762.

Brierley, A. S., and Cox, M. J. 2015. Fewer but not smaller schools in declining fish and krill populations. Current Biology, 25: 75–79.

Buskey, E. J. 1998. Energetic cost of position-holding behavior in the planktonic mysid *Mysidium columbiae*. Marine Ecology Progress Series, 172: 139–147.

Catton, K. B., Webster, D. R., Kawaguchi, S., and Yen, J. 2011. The hydrodynamic disturbances of two species of krill: implications for aggregation structure. Journal of Experimental Biology, 214: 1845–1856.

CCAMLR. 2005. Report of the first meeting of the subgroup on acoustic survey and analysis methods. SC-CCAMLR-XXIV/BG/3.

Coetzee, J. 2000. Use of a shoal analysis and patch estimation system (SHAPES) to characterize sardine schools. Aquatic Living Resources, 13: 1–10.

Cresswell, K. A., Tarling, G. A., and Trathan, P. N. 2007. Weight loss during breeding is adaptive for female macaroni penguins, *Eudyptes chrysolophus*. Evolutionary Ecology Research, 9: 1053–1076.

Croxall, J. P., Everson, I., Kooyman, G. L., Ricketts, C., and Davis, R. W. 1985. Fur-seal diving behavior in relation to vertical distribution of krill. Journal of Animal Ecology, 54: 1–8.

Croxall, J. P., Reid, K., and Prince, P. A. 1999. Diet, provisioning and productivity responses of marine predators to differences in availability of Antarctic krill. Marine Ecology Progress Series, 177: 115–131.

Diner, N. 1998. Correction on school geometry and density: approach based on acoustic image simulation. ICES Conference and Meeting Documents, B:1. 51 pp.

Diner, N. 2001. Correction on school geometry and density: approach based on acoustic image simulation. Aquatic Living Resources, 14: 211–222.

Folt, C. 1987. An experimental analysis of costs and benefits of zooplankton aggregation. *In* Predation, Direct and Indirect Impacts on Aquatic Communities, pp. 300–314. Ed. by J. Benndorf. University Press of New England, Hanover and London. 386 pp.

Folt, C. L., and Burns, C. W. 1999. Biological drivers of zooplankton patchiness. Trends in Ecology & Evolution, 14: 300–305.

Foote, K. G., Everson, I., Watkins, J. L., and Bone, D. G. 1990. Target strength of Antarctic krill (*Euphausia superba*) at 38 and 120 kHz. Journal of the Acoustic Society of America, 87: 16–24.

Foote, K. G., Knudsen, F. R., Vestnes, G., MacLennan, D. N., and Simmonds, E. J. 1987. Calibration of acoustic instruments for fish density estimation: a practical guide. ICES Cooperative Research Report, 144. 69 pp.

Fréon, P., Gerlotto, F., and Soria, M. 1992. Changes in school structure according to external stimuli: description and influence on acoustic assessment. Fisheries Research, 15: 45–66.

Gordon, A. L., Georgi, D. T., and Taylor, H. W. 1977. Antarctic polar frontal zone in the western Scotia sea - summer 1975. Journal of Physical Oceanography, 7: 309–328.

Grünbaum, D., and Veit, R. R. 2003. Black-browed albatrosses foraging on Antarctic krill: density-dependence through local enhancement? Ecology, 84: 3265–3275.

Hamner, W. M. 1984. Aspects of schooling of *Euphausia superba*. Journal of Crustacean Biology, 4: 67–74.

Hamner, W. M., and Hamner, P. P. 2000. Behavior of Antarctic krill (*Euphausia superba*): schooling, foraging, and antipredatory behavior. Canadian Journal of Fisheries and Aquatic Sciences, 57: 192–202.

Hemelrijk, C. K., and Hildenbrandt, H. 2012. Schools of fish and flocks of birds: their shape and internal structure by self-organization. Interface Focus, 2: 726–737.

Hewitt, R. P., Watkins, J., Naganobu, M., Sushin, V., Brierley, A. S., Demer, D., Kasatkina, S., *et al.* 2004. Biomass of Antarctic krill in the Scotia Sea in January/February 2000 and its use in revising an estimate of precautionary yield. Deep-Sea Research Part II: Topical Studies in Oceanography, 51: 1215–1236.

Johnson, M. A., Macaulay, M. C., and Biggs, D. C. 1984. Respiration and excretion within a mass aggregation of *Euphausia superba*: implications for krill distribution. Journal of Crustacean Biology, 4: 174–184.

Kawaguchi, S., King, R., Meijers, R., Osborn, J. E., Swadling, K. M., Ritz, D. A., and Nicol, S. 2010. An experimental aquarium for observing the schooling behaviour of Antarctic krill (*Euphausia superba*). Deep-Sea Research Part II: Topical Studies in Oceanography, 57: 683–692.

Kils, U. 1981. Swimming behaviour, swimming performance and energy balance of Antarctic krill *Euphausia superba*. BIOMASS Scientific Series, 3: 1–121.

Klevjer, T. A., Tarling, G. A., and Fielding, S. 2010. Swarm characteristics of Antarctic krill *Euphausia superba* relative to the proximity of land during summer in the Scotia Sea. Marine Ecology Progress Series, 409: 157–170.

Korb, R. E., Whitehouse, M. J., Ward, P., Gordon, M., Venables, H. J., and Poulton, A. J. 2012. Regional and seasonal differences in microplankton biomass, productivity, and structure across the Scotia Sea: implications for the export of biogenic carbon. Deep-Sea Research Part II: Topical Studies in Oceanography, 59: 67–77.

Krafft, B. A., Skaret, G., Knutsen, T., Melle, W., Klevjer, T., and Soiland, H. 2012. Antarctic krill swarm characteristics in the Southeast Atlantic sector of the Southern Ocean. Marine Ecology Progress Series, 465: 69–83.

Lawson, G. L., Wiebe, P. H., Stanton, T. K., and Ashjian, C. J. 2008. Euphausiid distribution along the Western Antarctic Peninsula—Part A: development of robust multi-frequency acoustic techniques to identify euphausiid aggregations and quantify euphausiid size, abundance and biomass. Deep-Sea Research Part II: Topical Studies in Oceanography, 55: 412–431.

Makris, N. C., Ratilal, P., Symonds, D. T., Jagannathan, S., Lee, S., and Nero, R. W. 2006. Fish population and behavior revealed by instantaneous continental shelf-scale imaging. Science, 311: 660–663.

Murphy, E. J., Thorpe, S. E., Watkins, J. L., and Hewitt, R. 2004. Modeling the krill transport pathways in the Scotia Sea: spatial and environmental connections generating the seasonal distribution of krill. Deep-Sea Research Part II: Topical Studies in Oceanography, 51: 1435–1456.

Murphy, E. J., Watkins, J. L., Trathan, P. N., Reid, K., Meredith, M. P., Thorpe, S. E., Johnston, N. M., *et al.* 2007. Spatial and temporal operation of the Scotia Sea ecosystem: a review of large-scale links in a krill centred food web. Philosophical Transactions of the Royal Society B: Biological Sciences, 362: 113–148.

O'Brien, D. P. 1988. Surface schooling behavior of the coastal krill *Nyctiphanes australis* (Crustacea, Euphausiacea) off Tasmania, Australia. Marine Ecology Progress Series, 42: 219–233.

O'Brien, D. P. 1989. Analysis of the internal arrangement of individuals within crustacean aggregations (Euphausiacea, Mysidacea). Journal of Experimental Marine Biology and Ecology, 128: 1–30.

Parrish, J. K., and Edelstein-Keshet, L. 1999. Complexity, pattern and evolutionary trade-offs in animal aggregation. Science, 284: 99–101.

Pinel-Alloul, P. 1995. Spatial heterogeneity as a multiscale characteristic of zooplankton community. Hydrobiologia, 300: 17–42.

Rieucau, G., Fernö, A., Ioannou, C. C., and Handegard, N. O. 2015. Towards of a firmer explanation of large shoal formation, maintenance and collective reactions in marine fish. Reviews in Fish Biology and Fisheries, 25: 21–37.

Ritz, D. A., Foster, E. G., and Swadling, K. M. 2001. Benefits of swarming: mysids in larger swarms save energy. Journal of the Marine Biological Association of the United Kingdom, 81: 543–544.

Ritz, D. A., Hobday, A. J., Montgomery, J. C., and Ward, A. J. W. 2011. Social aggregation in the pelagic zone with special reference to fish and invertebrates. *In* Advances in Marine Biology, 60, pp. 161–227. Ed. by M. Lesser. Elsevier, Amsterdam. 272 pp.

Siegel, V., and Kalinowski, J. 1994. Krill demography and small-scale processes: a review. *In* Southern Ocean Ecology: The BIOMASS Perspective, pp. 145–164. Ed. by S. Z. El-Sayed. Cambridge University Press, Cambridge, England. 446 pp.

Swadling, K. M., Ritz, D. A., Nicol, S., Osborn, J. E., and Gurney, L. J. 2005. Respiration rate and cost of swimming for Antarctic krill, *Euphausia superba*, in large groups in the laboratory. Marine Biology, 146: 1169–1175.

Tarling, G. A. 2003. Sex-dependent diel vertical migration in northern krill *Meganyctiphanes norvegica* and its consequences for population dynamics. Marine Ecology Progress Series, 260: 173–188.

Tarling, G. A., Cuzin-Roudy, J., and Buchholz, F. 1999. Vertical migration behaviour in the northern krill *Meganyctiphanes norvegica* is influenced by moult and reproductive processes. Marine Ecology Progress Series, 190: 253–262.

Tarling, G. A., Klevjer, T., Fielding, S., Watkins, J. L., Atkinson, A., Murphy, E., Korb, R., *et al.* 2009. Variability and predictability of Antarctic krill swarm structure. Deep-Sea Research Part I: Oceanographic Research Papers, 56: 1994–2012.

Tarling, G. A., and Thorpe, S. E. 2014. Instantaneous movement of krill swarms in the Antarctic circumpolar current. Limnology and Oceanography, 59: 872–886.

Tarling, G. A., and Thorpe, S. E. 2017. Oceanic swarms of Antarctic krill perform satiation sinking. Proceedings of the Royal Society B: Biological Sciences, 284: 20172015.

Tarling, G. A., Thorpe, S. E., Fielding, S., Klevjer, T., Ryabov, A., and Somerfield, P. J. 2018. Varying depth and swarm dimensions of open-ocean Antarctic krill *Euphausia superba* Dana, 1850 (Euphausiacea) over diel cycles. Journal of Crustacean Biology, 38: 716–727.

Venables, H., Meredith, M. P., Atkinson, A., and Ward, P. 2012. Fronts and habitat zones in the Scotia Sea. Deep-Sea Research Part II: Topical Studies in Oceanography, 59: 14–24.

Watkins, J. L., and Brierley, A. S. 1996. A post-processing technique to remove background noise from echo integration data. ICES Journal of Marine Science, 53: 339–344.

Weber, L. H., El-Sayed, S. Z., and Hampton, I. 1986. The variance spectra of phytoplankton, krill and water temperature in the Antarctic Ocean, south of Africa. Deep Sea Research Part A: Oceanographic Research Papers, 33: 1327–1343.

Wiese, K. 1996. Sensory capacities of euphausiids in the context of schooling. Marine and Freshwater Behaviour and Physiology, 28: 183–194.

Woodd-Walker, R. S., Watkins, J. L., and Brierley, A. S. 2003. Identification of Southern Ocean acoustic targets using aggregation, backscatter and shape characteristics. ICES Journal of Marine Science, 60: 641–649.

Zhou, M., and Dorland, R. D. 2004. Aggregation and vertical migration behavior of *Euphausia superba*. Deep-Sea Research Part II: Topical Studies in Oceanography, 51: 2119–2137.

Zhou, M., Nordhausen, W., and Huntley, M. 1994. ADCP measurements of the distribution and abundance of euphausiids near the Antarctic Peninsula in winter. Deep-Sea Research Part I: Oceanographic Research Papers, 41: 1425–1445.

Handling editor: Howard Browman